


FULL PAPER

Open Access



Several outstanding issues concerning the ionosphere of Mars

Paul Withers^{1*} , Marianna Felici², Jennifer Segale¹, Elias Barbinis³, Danny Kahan³ and Kamal Oudrhiri³

Abstract

Several outstanding issues concerning the ionosphere of Mars can be addressed with the support of radio occultation observations acquired near the solar zenith angle limit of 45°. First, two fundamentally different types of instruments (topside radar sounding, radio occultations) have been used to characterize how the subsolar peak density changes over the solar cycle. Here we find that their results for solar minimum and solar maximum values of peak density are consistent. This verifies that systematic errors do not affect peak density measurements from either type of instrument. Second, reported descriptions of how the peak altitude changes with solar zenith angle are inconsistent. Specifically, values reported by radio occultation and radar sounder instruments for the characteristic lengthscale used to describe changes in peak altitude with solar zenith angle vary by a factor of two. We find that the change in peak altitude with solar zenith angle is governed by a lengthscale that is close to the thermospheric scale height, as predicted theoretically. However, this behavior is only apparent when the Mars–Sun distance is held fixed. Reported smaller values of this lengthscale, which are not consistent with theoretical expectations, were adversely affected by using near-terminator peak altitude values only, which display marked variability. Third, Viking Lander entry science data have been interpreted to suggest that the M1 layer is not present in the ionosphere at solar zenith angles of 45° or smaller. We show radio occultation observations at 45° in which the M1 layer is present. This suggests that the basic structure of the dayside ionosphere remains the same at all solar zenith angles.

Keywords Mars, Ionosphere, Radio occultation

*Correspondence:

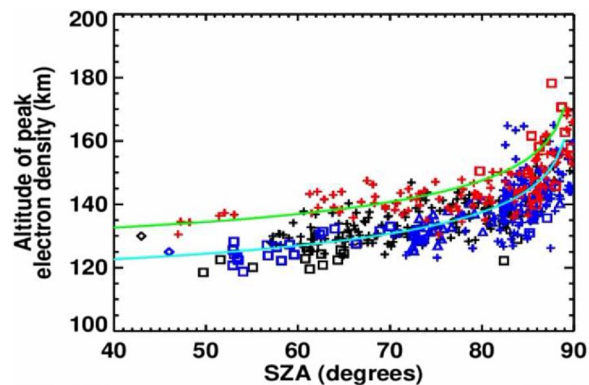
Paul Withers
withers@bu.edu

Full list of author information is available at the end of the article



© The Author(s) 2024. **Open Access** This article is licensed under a Creative Commons Attribution 4.0 International License, which permits use, sharing, adaptation, distribution and reproduction in any medium or format, as long as you give appropriate credit to the original author(s) and the source, provide a link to the Creative Commons licence, and indicate if changes were made. The images or other third party material in this article are included in the article's Creative Commons licence, unless indicated otherwise in a credit line to the material. If material is not included in the article's Creative Commons licence and your intended use is not permitted by statutory regulation or exceeds the permitted use, you will need to obtain permission directly from the copyright holder. To view a copy of this licence, visit <http://creativecommons.org/licenses/by/4.0/>.

Graphical Abstract



1 Introduction

The ionosphere of Mars is a region of thermal plasma of planetary origin (i.e., as opposed to solar wind origin) that is found within and above the planet's upper atmosphere (Barth et al. 1992; Withers 2009; Bougher et al. 2017; Bauer and Lammer 2004; Witasse et al. 2008; Schunk and Nagy 2009; González-Galindo 2020). Dayside ionospheric densities depend strongly on solar zenith angle (e.g., Hantsch and Bauer 1990; Zhang et al. 1990; Barth et al. 1992; Nielsen et al. 2006; Fox and Yeager 2006, 2009; Morgan et al. 2008; Withers 2009; Němec et al. 2011; Bougher et al. 2017; Peter et al. 2014, 2021, 2023). They are greatest near the subsolar point and decrease smoothly with increasing solar zenith angle. Terminator densities are approximately one order of magnitude smaller than subsolar densities. Dayside ionospheric densities also increase as the ionizing solar irradiance increases over the solar cycle (e.g., Stewart and Hanson 1982; Hantsch and Bauer 1990; Němec et al. 2011; Withers et al. 2015a).

The vertical structure of the dayside ionosphere of Mars is generally considered to be dominated by two layers (Barth et al. 1992; Withers 2009; Bougher et al. 2017; Bauer and Lammer 2004; Witasse et al. 2008; Schunk and Nagy 2009). The upper M2 layer is more dense. Here the source of plasma is primarily photoionization of atmospheric species by solar extreme ultraviolet (EUV) photons at 15–90 nm. The lower M1 layer is less dense, typically about 40% as dense as the M2 layer (Fox and Yeager 2006, 2009; Fallows et al. 2015). Here the source of plasma is primarily photoionization of atmospheric species by solar soft X-ray photons at 1–15 nm, although this is strongly amplified by associated electron impact ionization (e.g., Simon Wedlund et al. 2011; Fallows et al. 2015).

The fundamental physical and chemical processes responsible for these two ionospheric layers operate similarly on Venus, which also has a CO₂-dominated atmosphere in which O is an important secondary component (Bauer and Lammer 2004; Witasse et al. 2008; Schunk and Nagy 2009). Consequently, comparisons of Mars's ionosphere to Venus's ionosphere (e.g., Cravens et al. 1981; Kliore 1992; Luhmann et al. 1992; Fox and Kliore 1997; Peter et al. 2014; Girazian et al. 2015; Hensley and Withers 2021; Ambili et al. 2022; Tripathi et al. 2023; Ambili et al. 2024) can advance understanding of both objects and of general principles that govern ionospheres.

The vertical structure of the dayside ionosphere provides multiple useful indications of how the ionosphere behaves. The value of the maximum density in the M2 layer, commonly known as the peak density, characterizes the total amount of plasma present in the ionosphere (e.g., Withers 2009; Schunk and Nagy 2009; Bougher et al. 2017). The corresponding altitude, commonly known as the peak altitude, indicates the extent to which ion–neutral interactions (e.g., reactions, collisions) may influence ionospheric behavior. Interactions are greater when the neutral atmosphere is denser. Consequently, many studies have used peak density and peak altitude to characterize the distribution of plasma in the ionosphere (e.g., Hantsch and Bauer 1990; Zhang et al. 1990; Nielsen et al. 2006; Fox and Yeager 2006, 2009; Morgan et al. 2008; Němec et al. 2011; Fallows et al. 2015; Peter et al. 2014, 2021, 2023).

Many of these previous studies have examined how the peak density and peak altitude change with factors such as solar irradiance, solar zenith angle, and Mars–Sun distance. However, several notable issues concerning the

dependence of ionospheric properties on these factors remain unresolved.

Two fundamentally different types of instruments (topside radar sounding, radio occultations) have been used to characterize how the subsolar peak density changes over the solar cycle (e.g., Stewart and Hanson 1982; Hantsch and Bauer 1990; Fox and Yeager 2009; Němec et al. 2011; Chen et al. 2023). However, previous studies have not fully addressed whether results for different instrument types are consistent, which is important for testing whether either instrument type is subject to systematic errors. Here we test whether topside radar sounding and radio occultations provide consistent results for how the subsolar peak density changes over the solar cycle.

Many previous studies have used ionospheric observations to infer a representative value for the subsolar peak altitude and to characterize how the peak altitude changes with solar zenith angle (e.g., Hantsch and Bauer 1990; Zhang et al. 1990; Nielsen et al. 2006; Fox and Yeager 2006, 2009; Morgan et al. 2008; Němec et al. 2011; Fallows et al. 2015). Reported descriptions of how the peak altitude changes with solar zenith angle are inconsistent. Specifically, reported values of the characteristic lengthscale used to describe changes in peak altitude with solar zenith angle vary by a factor of two. Values at the larger end of the range are consistent with theoretical expectations, whereas values at the smaller end of the range are not. Here we examine whether reported small lengthscales are reliable and, if so, how they should be physically interpreted.

The M1 layer is less well-studied than the M2 layer (e.g., Liao et al. 2006; Fox and Yeager 2006, 2009; Fox and Weber 2012; Fallows et al. 2015; Yao et al. 2019). In fact, it is debated whether the M1 layer is present at small solar zenith angles or not (Mayyasi and Mendillo 2015). Here we address that question.

Addressing these three issues will advance understanding of the behavior of the dayside ionosphere at Mars. We do so here by analysis of radio occultation observations from Mariner 9, Viking Orbiters 1 and 2, and MAVEN. This is supported by the incorporation of results from earlier studies that used these datasets, radio occultation observations from Mars Global Surveyor (MGS), and topside radar sounder observations from the MARSIS instrument on Mars Express.

The structure of this article is as follows. Section 2 describes the radio occultation observations from Mariner 9, Viking Orbiters 1 and 2, and MAVEN that are used in this work. Section 3 investigates peak electron density. Section 4 investigates peak altitude. Section 5

investigates the M1 layer. Section 6 presents the conclusions of this work.

2 Data

Several different types of instruments have acquired measurements of densities in the ionosphere of Mars. The main types are radio occultations, which have been conducted by many spacecraft, topside radar sounding, which has been conducted by the MARSIS instrument on Mars Express, and in situ observations, which have been acquired by MAVEN and the two Viking Landers (Barth et al. 1992; Withers 2009; Haider et al. 2011; Bougher et al. 2017; González-Galindo 2020).

Radio occultations yield vertical profiles of ionospheric electron density (e.g., Kliore 1992; Hinson et al. 1999; Pätzold et al. 2016; Withers et al. 2020a). Such profiles are typically characterized by excellent vertical range, vertical resolution, and electron density uncertainty. However, geometric constraints limit radio occultation observations at Mars to solar zenith angles between 45° and 135° (e.g., Tamburo et al. 2023). Moreover, due to the inherent nature of limb sounding experiments, radio occultation observations may be distorted if the ionosphere is not spherically symmetric on the horizontal lengthscales of interest, which are a few hundred kilometers (Hinson et al. 1999).

Topside radar sounding by the MARSIS instrument on the Mars Express spacecraft is able to access all solar zenith angles (Gurnett et al. 2005, 2008; Morgan et al. 2008; Němec et al. 2011). However, its derived vertical profiles have relatively poor vertical resolution and relatively poor absolute accuracy in reported altitudes (Morgan et al. 2013). This is due to the 91.4 microsecond time resolution of the instrument. Radio waves travel 27 km in this time, which for two-way ranging results in altitude uncertainties of at least ± 7 km (Nielsen 2004; Morgan et al. 2008, 2013). Furthermore, these profiles are limited to altitudes above the peak altitude.

In situ measurements by various instruments on MAVEN are also able to access all solar zenith angles (e.g., Jakosky et al. 2015; Bougher et al. 2015; Benna et al. 2015; Mendillo et al. 2017). However, such measurements are limited to altitudes above the spacecraft periapsis. MAVEN's periapsis is generally around 150 km altitude with limited excursions to 120 km altitude during sporadic Deep Dip campaigns (Jakosky et al. 2015; Stone et al. 2022).

MARSIS provides valuable measurements of ionospheric peak density that have been comprehensively examined in previous work. We do not repeat those studies here, instead extensively incorporating their findings into our discussions and interpretations. We note that, in general, it is valuable to compare radio

occultation studies and MARSIS studies in order to verify that findings are robust and reproducible. That is, that they are not influenced by an unsuspected bias or error in either type of instrument. MARSIS measurements of peak altitude are much less accurate than those available from other instruments, so they are not used heavily here. MARSIS cannot sample the M1 layer, so its observations cannot support studies of the M1 layer.

Few studies of ionospheric peak density and peak altitude have used MAVEN in situ measurements (Vogt et al. 2017). Those studies did not address the issues raised here. Due to MAVEN's periapsis altitude, which is relatively high even during Deep Dips, no in situ measurements of the M1 layer have been reported. In addition to MAVEN, each of the two Viking Landers acquired one vertical profile of ionospheric densities during its descent. They are used frequently in this article.

Therefore, we analyze radio occultation observations to address the aims of this article. Specifically, we use radio occultation observations from Mariner 9, Viking Orbiters 1 and 2, and MAVEN. Many similar observations are available from MGS. However, as they are restricted to solar zenith angles greater than 70° , they are not used directly in this article. Nevertheless, we incorporate published findings from previous analyses of MGS profiles into our discussions and interpretations where appropriate. Similar radio occultation observations have been acquired by other spacecraft, but they are not used here as they are not yet available in open archives.

We next present brief summaries of the characteristics of radio occultation observations from Mariner 9, Viking Orbiters 1 and 2, and MAVEN. As results obtained from similar observations by MGS are referred to extensively throughout this article, we also summarize the characteristics of that dataset as well.

Mariner 9 conducted two-way radio occultation observations at S-band in 1971–1972 (Kliore et al. 1972, 1973; Withers et al. 2015b). Ionospheric electron density profiles were obtained for ingress observations that occurred on the dayside. Solar zenith angles as small as 47° were sampled. Seventy-eight profiles were acquired during the primary mission on orbits 1–79 (solar zenith angles of 47° – 57°) and 36 profiles were acquired during the extended mission on orbits 352–450 (solar zenith angles of 72° – 99°). In the primary mission, profiles typically spanned 80 to 300 km with a vertical resolution of 2 km and a lowest reported density of $7 \times 10^8 \text{ m}^{-3}$, which can be considered to be a proxy for electron density uncertainty. In the extended mission, profiles typically spanned 80 to 240 km with a vertical resolution of 1 km and a lowest reported density of $1.2 \times 10^9 \text{ m}^{-3}$. The primary mission profiles were acquired as a

tremendous dust storm raged on Mars. The ionospheric peak was 20–30 km higher during this storm than normal (Hantsch and Bauer 1990), indicating significant expansion of the lower atmosphere due to suspended dust during this immense dust storm. In this work, we exclude Mariner 9 profiles at solar zenith angles greater than 90° . As discussed in Withers et al. (2015b), we also exclude the profile observed on orbit 4, which leaves 110 Mariner 9 profiles available for analysis.

Viking Orbiters 1 and 2 conducted coherent dual-frequency radio occultation observations at S-band and X-band in 1976–1978, where the two coherent downlinked radio signals were both referenced to an S-band uplink signal (Lindal et al. 1979; Kliore 1992; Withers et al. 2020b). Solar zenith angles as small as 50° were sampled. Sixty-nine profiles spanning solar zenith angles of 50° – 95° are preserved and deemed suitable for scientific analysis (Withers et al. 2020b). Most of these profiles are from ingress occultations, only three were from egress occultations. The characteristic electron density uncertainty in these profiles is $2 \times 10^9 \text{ m}^{-3}$. In this work, we exclude Viking Orbiter profiles at solar zenith angles greater than 90° , which leaves 60 Viking Orbiter profiles available for analysis.

The MAVEN Radio Occultation Science Experiment (ROSE) has conducted two-way radio occultation observations at X-band since 2016 (Withers et al. 2020a, 2022, 2023; Felici et al. 2020, 2022). At the time of writing, ROSE has archived 1228 profiles and continues to acquire new observations. Solar zenith angles as small as 47° have been sampled. ROSE profiles from July–October 2016, February 2017, and June–August 2018 were acquired during dust events (Withers et al. 2018; Felici et al. 2020). As for Mariner 9, the ionospheric peak in those profiles was noticeably higher in altitude than usual. The characteristic electron density uncertainty in these profiles is 2 – $3 \times 10^9 \text{ m}^{-3}$ (Withers et al. 2020a). In this work, we exclude MAVEN ROSE profiles at solar zenith angles greater than 90° . In order to ensure that the inferred peak properties are representative of underlying ionospheric conditions, we require that the profile has a full vertical extent. Specifically, we require that it span altitudes from 100 km to 200 km. We also exclude profiles acquired on egress occultations. As will be discussed in a forthcoming publication, the data processing pipeline for egress occultations is currently being improved, which will lead to revisions in the archived egress profiles. Finally, we exclude three noisy near-terminator profiles where excessive scatter in derived electron density values results in the largest electron density value occurring above 250 km, which is clearly not representative of the dayside ionospheric peak. This leaves 424 MAVEN ROSE profiles available for analysis.

MGS conducted one-way radio occultation observations at X-band in 1998–2005 (Hinson et al. 1999; Tyler et al. 2001; Withers et al. 2008). 5600 profiles spanning solar zenith angles of 71.0°–89.2° were generated. With the exception of 220 profiles at southern latitudes of 69.1°S to 64.6°S, all profiles were acquired at high northern latitudes of 60.6°N to 85.5°N. The characteristic electron density uncertainty in these profiles is $4.6 \times 10^9 \text{ m}^{-3}$. As the first significant ionospheric dataset acquired since the Viking epoch, these profiles have been widely used in previous work.

3 Peak electron density

Many previous works have reported values for the subsolar peak density (e.g., Stewart and Hanson 1982; Hantsch and Bauer 1990; Zhang et al. 1990; Nielsen et al. 2006; Fox and Yeager 2006; Morgan et al. 2008; Fox and Yeager 2009; Němec et al. 2011; Fallows et al. 2015; Yao et al. 2019; Chen et al. 2023) and most of them have also assessed how subsolar peak density changes with ionizing solar irradiance. They provide a suite of predictions for subsolar peak density under solar minimum and solar maximum conditions. These studies have generally used one of two possible types of data: MARSIS and radio occultation observations. Testing whether results from these two instrument types agree is important for verifying that neither instrument type suffers from systematic errors (e.g., Morgan et al. 2008; Vogt et al. 2016).

Němec et al. (2011) conducted a comprehensive analysis of MARSIS observations of peak density. Equation 6 of Němec et al. (2011) predicts how subsolar peak density changes with the F10.7 proxy for ionizing solar irradiance. Predicted values are $1.53 \times 10^{11} \text{ m}^{-3}$ for F10.7=70 (solar minimum), $1.88 \times 10^{11} \text{ m}^{-3}$ for F10.7=120 (solar moderate), and $2.30 \times 10^{11} \text{ m}^{-3}$ for F10.7=200 (solar maximum). As the relationships developed by Němec et al. (2011) incorporated a dependence on Mars–Sun distance, the orbital semi-major axis of 1.524 AU was used to generate these numerical values.

We compare these predictions from MARSIS directly against radio occultation observations. The top panel of Fig. 1 shows the dependence of peak electron density on solar zenith angle. The general trend of decreasing peak electron density with increasing solar zenith angle is readily apparent.

The top panel of Fig. 1 also shows the peak total ion density values measured by the two Viking Landers during their descents on 20 July 1976 (Viking Lander 1, solar zenith angle of 44°) and 03 September 1976 (Viking Lander 2, solar zenith angle of 45°). The solar zenith

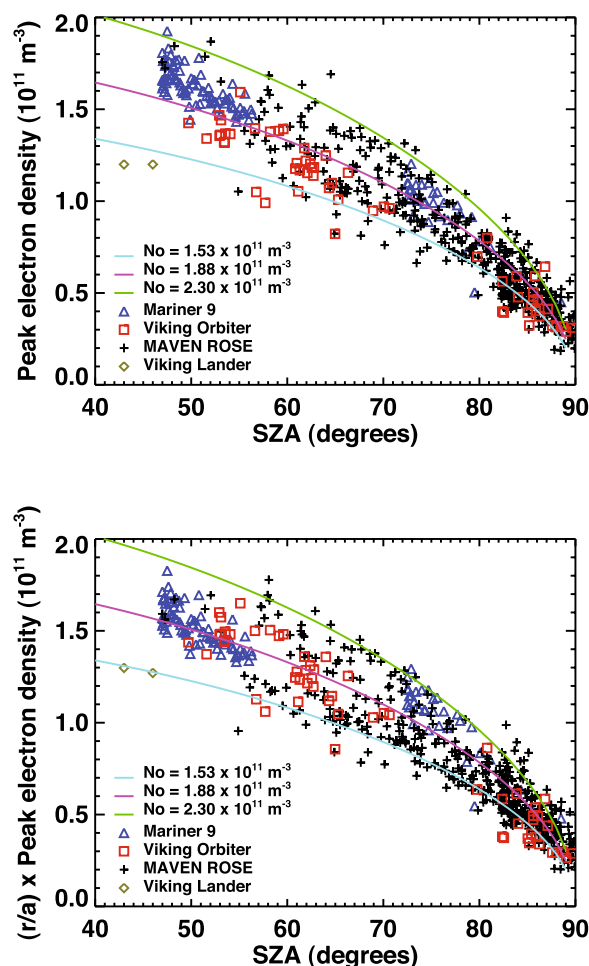


Fig. 1 (Top) Dependence of observed peak electron density values on solar zenith angle. Mariner 9 values are shown by blue triangles, Viking Orbiter values are shown by red squares, MAVEN ROSE values are shown by black crosses, and Viking Lander values are shown by olive green diamonds. The three lines are illustrative indications of how peak electron density changes with solar zenith angle, each with a different subsolar value. The cyan line has $N_0 = 1.53 \times 10^{11} \text{ m}^{-3}$, the magenta line has $N_0 = 1.88 \times 10^{11} \text{ m}^{-3}$, and the green line has $N_0 = 2.30 \times 10^{11} \text{ m}^{-3}$. (bottom) As top panel, but for adjusted peak electron density values where r is Mars–Sun distance and a is the semi-major axis distance of 1.524 AU

angle at the spacecraft changed with altitude during each descent through the ionosphere as neither trajectory was perfectly vertical (Hanson et al. 1977); in this work, we have adopted values appropriate for the altitude of the ionospheric peak. For these months, the average value of F10.7 was 70. We adopt the peak density values of $1.2 \times 10^{11} \text{ m}^{-3}$ shown in Figure 1 of Hantsch and Bauer (1990).

Useful lower limits on the subsolar peak density are provided by observations at solar zenith angles near 45°.

The densities of the main ionospheric layers vary as the square root of the cosine of solar zenith angle (Hantsch and Bauer 1990; Zhang et al. 1990; Nielsen et al. 2006; Fox and Yeager 2006, 2009; Morgan et al. 2008; Němec et al. 2011; Peter et al. 2014, 2021, 2023), such that their densities at a solar zenith angle of 45° are approximately 85% of their subsolar values. There are 39 Mariner 9 observations at solar zenith angles less than 50° . These were acquired in December 1971, when the monthly average value of F10.7, a common proxy for ionizing solar irradiance, was 120. The corresponding peak electron density values span from $1.4 \times 10^{11} \text{ m}^{-3}$ to $1.9 \times 10^{11} \text{ m}^{-3}$ and their average value is $1.7 \times 10^{11} \text{ m}^{-3}$. There is 1 Viking orbiter observation at solar zenith angles less than 50° . This was acquired on 20 October 1977, when the monthly average value of F10.7 was 100, at a solar zenith angle of 49.7° . The corresponding peak electron density value is $1.4 \times 10^{11} \text{ m}^{-3}$. There are 3 MAVEN ROSE observations at solar zenith angles less than 50° . These were acquired on 13, 15, and 16 June 2022, when the monthly average value of F10.7 was 120. The corresponding peak electron density values are $1.8 \times 10^{11} \text{ m}^{-3}$. The two Viking Lander observations summarized above are also relevant here.

The MAVEN ROSE peak densities at F10.7=120 are slightly greater than the Mariner 9 peak densities at the same irradiance level. While we make no claims that this is statistically significant, it is consistent with Mars being closer to the Sun for the MAVEN ROSE observations around $L_s=250^\circ$ than for the Mariner 9 observations around $L_s=310^\circ$.

It follows that these peak densities observed at solar zenith angles near 45° , which are listed in Table 1, are only slightly smaller than the subsolar peak densities that were present on Mars at the times of the observations. The dependence of peak electron density on ionizing solar irradiance, as represented by the F10.7 proxy, is apparent in these results. The projected values of subsolar peak density listed in Table 1 are broadly consistent with the results of Němec et al. (2011). The empirical model of Němec et al. (2011) predicted values of subsolar peak density of $1.53 \times 10^{11} \text{ m}^{-3}$ for F10.7=70

(solar minimum), $1.88 \times 10^{11} \text{ m}^{-3}$ for F10.7=120 (solar moderate), and $2.30 \times 10^{11} \text{ m}^{-3}$ for F10.7=200 (solar maximum).

This approach is formalized in the top panel of Fig. 1, which also shows several illustrative indications of how peak electron density changes with solar zenith angle. These lines, which are not fits to the data points, satisfy $N_m(\chi) = N_0 \cos^{0.5} \chi$, where N_m is peak electron density, N_0 is the subsolar peak electron density, and χ is solar zenith angle (e.g., Withers 2009). Following Němec et al. (2011), the three lines shown in the top panel of Fig. 1 use values of 1.53, 1.88, and $2.30 \times 10^{11} \text{ m}^{-3}$ for N_0 . The MARSIS observations from which these lines were generated are shown in Figure 3a of Němec et al. (2011). It is clear that the three lines represent the observations well. The flanking lines, where N_0 equals 1.53 and $2.30 \times 10^{11} \text{ m}^{-3}$, track the edges of the envelope of radio occultation peak electron density values. The intermediate line, where N_0 equals $1.88 \times 10^{11} \text{ m}^{-3}$, traces through the center of the set of radio occultation peak electron density values. This comparison illustrates that peak electron density values obtained from MARSIS and radio occultation observations are consistent. That is, there are no indications of a systematic error in either instrument type.

The Viking Lander densities seem unusually low relative to other observations made at similar solar zenith angles in the top panel of Fig. 1 and, indeed, were questioned on that basis by Hantsch and Bauer (1990) in their impactful study of solar control of the Martian ionosphere. Due to the centrality of the Viking Lander ion density profiles in essentially all studies of the Mars ionosphere in the two decades between Viking and MGS, the consequences of a significant error in the absolute values of these densities would be profound. However, these densities, which were measured when solar irradiance was low and the F10.7 value was 70, lie close to the lower line in the top panel of Fig. 1. Furthermore, these densities are consistent with comparable MARSIS observations. These Viking Lander values of $1.2 \times 10^{10} \text{ m}^{-3}$ at solar zenith angle around 45° imply corresponding subsolar peak density values of $1.4 \times 10^{10} \text{ m}^{-3}$. This is close to the benchmark solar minimum value from Němec et al. (2011) of $1.53 \times 10^{11} \text{ m}^{-3}$ that is discussed above. Moreover, it is also close to the lower quartile value of subsolar peak density of $1.45 \times 10^{10} \text{ m}^{-3}$ that was reported by Němec et al. (2011). Therefore, the Viking Lander densities are consistent with other observations of the ionosphere at solar minimum conditions. We conclude that the seemingly small peak electron density values measured by the two Viking Landers are appropriate for the very low levels of ionizing solar irradiance at the times of these observations. They are not unusual.

Table 1 Values of peak density from observations at solar zenith angles around 45°

Spacecraft	F10.7	Observed peak density (m^{-3})	Subsolar peak density (m^{-3})	Number of observations
Viking landers	70	1.2×10^{11}	1.4×10^{11}	2
Viking orbiters	100	1.4×10^{11}	1.7×10^{11}	1
Mariner 9	120	1.7×10^{11}	2.0×10^{11}	39
MAVEN ROSE	120	1.8×10^{11}	2.1×10^{11}	3

The results and interpretations obtained from the top panel of Fig. 1 are based on data acquired at various Mars–Sun distances. As the ionizing solar irradiance is inversely proportional to the square of the Mars–Sun distance and ionospheric densities are proportional to the square root of the ionizing irradiance (Bauer and Lammer 2004; Schunk and Nagy 2009), use of data at various Mars–Sun distances might introduce biases. To exclude this possibility, we make use of the concept that ionospheric densities should therefore be inversely proportional to Mars–Sun distance (Němec et al. 2011, 2019; Mendillo et al. 2018). We apply this relationship to adjust the peak electron density values shown in the top panel of Fig. 1 to a common Mars–Sun distance of 1.524 AU, which is the orbital semi-major axis. The adjusted peak electron density values are shown in the bottom panel of Fig. 1. The fine-scale details differ between the two panels, but the interpretations presented above are unchanged. One salient outcome of this adjustment concerns the two Viking Lander values, which were obtained at $L_s=97^\circ$ and $L_s=118^\circ$, close to aphelion at $L_s=71^\circ$. In the top panel of Fig. 1, they lie just below the lower line that represents solar minimum. However, in the bottom panel of Fig. 1, they lie on this line. The Viking Lander profiles were acquired around aphelion and under solar minimum conditions, so they reflect the lowest levels of ionizing solar irradiance that Mars can experience. It is hardly surprising that Hantsch and Bauer (1990) considered these values to be remarkably small in comparison to other observations.

Peak density values shown in the bottom panel of Fig. 1 still exhibit scatter at fixed solar zenith angle despite being adjusted to a common Mars–Sun distance. As most of the data points are confined between the lines representing solar minimum and solar maximum, it seems likely that inherent variations in the Sun’s ionizing irradiance with time make a significant contribution to this scatter.

In summary, radio occultation observations are consistent with MARSIS in that the subsolar peak electron density ranges between $1.53 \times 10^{11} \text{ m}^{-3}$ at solar minimum and $2.30 \times 10^{11} \text{ m}^{-3}$ at solar maximum. Also, contrary to earlier concerns, the seemingly small peak electron density values measured by the two Viking Landers are appropriate for the very low levels of ionizing solar irradiance present at the times of these observations.

4 Peak altitude

The relationship $z_m(\chi) = z_0 - L \ln \cos \chi$ has been used extensively to characterize the subsolar peak altitude and the dependence of peak altitude on solar zenith angle. Here z_m is peak altitude, z_0 is the subsolar peak altitude,

and L is a lengthscale. In idealized theory, the lengthscale L equals the neutral scale height H . A diverse range of values for z_0 and L has been reported by previous studies (e.g., Hantsch and Bauer 1990; Zhang et al. 1990; Nielsen et al. 2006; Fox and Yeager 2006, 2009; Morgan et al. 2008; Němec et al. 2011; Fallows et al. 2015). Reported values of z_0 generally range between 120 km and 130 km. This 10 km difference in z_0 is significant. It is equivalent to one neutral scale height or a factor of 3 in pressure (Withers 2006; Zurek et al. 2017; Stone et al. 2018). Reported values of L range between 5 km and 10 km. The implications of this factor-of-two difference in L are extremely impactful.

If $L = 5$ km, then the predicted ionospheric peak altitude increases by only 3.5 km from the subsolar point to a solar zenith angle of 60° . It increases by less than 2 km to a solar zenith angle of 45° . This predicted increase of a few km increase is modest. The variability in repeated observations of peak altitude under similar conditions is greater than this (e.g., Bougher et al. 2001, 2004). Consequently, if $L = 5$ km, then it implies that the ionospheric peak altitude is practically insensitive to changes in solar zenith angle below 60° . This is seen at Venus (Cravens et al. 1981; Girazian et al. 2015). If $L = 5$ km, then direct measurements of the subsolar peak altitude can effectively be obtained from radio occultation observations at solar zenith angles below 60° . Furthermore, the case in which $L = 5$ km is not consistent with idealized theory. This predicts that L should equal the thermospheric scale height H of around 10 km. That is, if $L = 5$ km, then the observed dependence of peak altitude on solar zenith angle would not have a theoretical explanation. This would imply a troubling lack of understanding of the fundamentals of the thermosphere–ionosphere system.

Conversely, if $L = 10$ km, then the predicted ionospheric peak altitude increases by 7 km from the subsolar point to a solar zenith angle of 60° . This is almost one neutral scale height. In this case, the rate of change of peak altitude with solar zenith angle is predicted correctly by idealized theory (i.e., L equals H).

In principle, MARSIS observations of peak altitude at all solar zenith angles, including at the subsolar point, should provide a complementary perspective that can help to clarify this picture. However, the process of determining ionospheric peak altitude from a MARSIS ionogram is complicated and dependent on a significant set of assumptions (Morgan et al. 2013; Němec et al. 2016). In addition, the relatively coarse time resolution of the instrument (91.4 microseconds) corresponds to an inherent altitude resolution of 14 km, which is large (Nielsen 2004; Morgan et al. 2008, 2013). Two separate studies of peak altitude by the MARSIS team have yielded divergent

results for subsolar peak altitude— 133.6 ± 0.1 km from Morgan et al. (2008) and 124.7 ± 0.1 km from Němec et al. (2011). These reported values differ by almost 9 km, yet both have uncertainties of 0.1 km. Finally, both those studies occurred before the discovery of an instrumental timing error (Golden-Marx et al. 2021). Their reported values for subsolar peak altitude should be increased by 13 km, which would introduce striking tension between the MARSIS peak altitudes and the radio occultation peak altitudes. We do not attempt to resolve that tension here, which might be influenced by the altitude resolution being an order of magnitude coarser for the MARSIS instrument than for radio occultation observations. Here we focus on discussion and interpretation of peak altitude values from radio occultation observations.

The top panel of Fig. 2 shows the dependence of peak altitude on solar zenith angle. The general trend of increasing peak altitude with increasing solar zenith angle is readily apparent.

The top panel of Fig. 2 also shows two illustrative indications of how peak altitude changes with solar zenith angle. These lines, which are not fits to data, satisfy $z_m(\chi) = z_0 - L \ln \cos \chi$, where z_m is peak altitude, z_0 is the subsolar peak altitude, and L is a lengthscale (e.g., Withers 2009). One line (cyan) uses $z_0 = 120$ km and $L = 10$ km, and the other line (magenta) uses $z_0 = 130$ km and $L = 5$ km. These two illustrative lines encompass the diverse range of parameter values determined by previous studies (e.g., Hantsch and Bauer 1990; Zhang et al. 1990; Nielsen et al. 2006; Fox and Yeager 2006, 2009; Morgan et al. 2008; Němec et al. 2011; Fallows et al. 2015). Each line seems to represent a subset of the observations well. The cyan line with $z_0 = 120$ km and $L = 10$ km, where the lengthscale L is comparable to the neutral scale height H as theoretically expected, represents the Mariner 9 extended mission data (solar zenith angles greater than 72°), the Viking Orbiter data, and the Viking Lander data well. This implies a relatively low subsolar peak altitude of 120 km. As discussed above, peak altitudes from the Mariner 9 primary mission (solar zenith angles less than 57°) were significantly elevated by a major global dust storm. On the other hand, the magenta line with $z_0 = 130$ km and $L = 5$ km, where the lengthscale L is significantly smaller than the neutral scale height H , represents most of the MAVEN ROSE data well. It does not represent MAVEN ROSE data acquired during dust storms, when peak altitude is atypically elevated, well (observations from July–October 2016, February 2017, and June–August 2018 at solar zenith angles less than 60° in which the peak altitude is greater than 140 km). Moreover, as shown in Fallows et al. (2015), $z_0 = 130$ km and $L = 5$ km also successfully represent the abundant set of MGS radio occultation observations, which are limited to solar

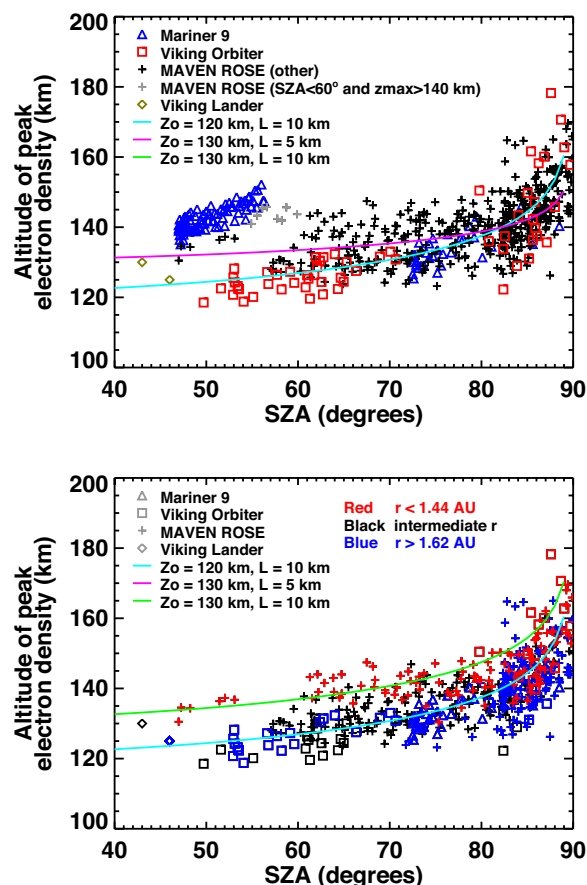


Fig. 2 (Top) Dependence of observed peak altitude values on solar zenith angle. Data points are indicated as in Fig. 1, with the exception of all MAVEN ROSE observations at solar zenith angles less than 60° that have peak altitudes greater than 140 km. Those MAVEN ROSE data points, which are affected by a dust storm, are shown by grey, not black, crosses. The two lines are illustrative indications of how peak altitude changes with solar zenith angle. The cyan line has z_0 of 120 km and L of 10 km, and the magenta line has z_0 of 130 km and L of 5 km. (bottom) Dependence of observed peak altitude values on solar zenith angle and Mars–Sun distance, excluding values severely affected by dust storms. Symbol shapes indicate spacecraft as in the top panel. Symbol color indicates Mars–Sun distance. Red indicates distances less than 1.44 AU, blue indicates distances greater than 1.62 AU, and black indicates intermediate distances. The cyan line has z_0 of 120 km and L of 10 km, as in the top panel, and the green line has z_0 of 130 km and L of 10 km

zenith angles between 70° and 90° . As discussed above, these two illustrative lines, although visually similar on the top panel of Fig. 2, present strikingly different pictures for the behavior of the dayside ionosphere.

MARSIS observations have provided a critical insight that can explain why previous studies of the behavior of the ionospheric peak altitude have yielded strikingly different results (z_0 values that differ by one scale height, L values that differ by a factor of two). Němec et al. (2011)

surveyed 30,283 MARSIS observations and deduced that the peak altitude decreases with increasing Mars–Sun distance. They interpreted this effect as being caused by greater thermal expansion of the atmosphere at smaller Mars–Sun distances. This may be a combination of direct and indirect behaviors: larger solar irradiance at smaller Mars–Sun distances (direct) and greater atmospheric dust loading at seasons close to perihelion (indirect). Their results suggest that the ionospheric peak altitude is 15 km higher at perihelion than at aphelion. Peter et al. (2023) used Mars Express radio occultation observations to examine ionospheric peak altitudes at solar zenith angles greater than 50° . They also found a dependence on Mars–Sun distance, with the ionospheric peak altitude being 15–20 km higher at perihelion than at aphelion. Finally, Mukundan et al. (2022) reported that a regional dust storm in 2016 was associated with an unexpectedly large increase of 20 km in peak altitude. They concluded that the occurrence of perihelion during this period contributed towards the magnitude of this large increase in peak altitude.

The bottom panel of Fig. 2 shows that Mariner 9, Viking Orbiter, Viking Lander, and MAVEN ROSE observations of peak altitude are similarly affected by the Mars–Sun distance. Observations noted above as being affected by dust storms, which are non-representative, are omitted from this panel. Following Peter et al. (2023), observations are classified as low, moderate, and high Mars–Sun distances, where distances less than 1.44 AU are classified as low, distances greater than 1.62 AU are classified as high, and intermediate distances are classified as moderate. There is considerable scatter in the observations, but they are broadly consistent with the notion that, at fixed solar zenith angle, ionospheric peak altitude decreases with increasing Mars–Sun distance. Two illustrative lines are shown. Both have $L = 10$ km, but one has $z_0 = 120$ km and the other has $z_0 = 130$ km. The upper green line ($z_0 = 130$ km) represents the low Mars–Sun distance observations reasonably well, at least at solar zenith angles less than 75° , and the lower cyan line ($z_0 = 120$ km) represents the high Mars–Sun distance observations reasonably well. This is reassuring—observations at fixed Mars–Sun distance can be represented by scenarios in which the lengthscale L equals the thermospheric scale height H , as expected from theoretical considerations.

This suggests a possible explanation for the disconcertingly small values of L that have been reported in previous studies (Fox and Weber 2012; Fallows et al. 2015). If those studies were based on datasets in which solar zenith angle is correlated with Mars–Sun distance, then this could have introduced bias into the results. For instance, if observations at large solar zenith angles

have high Mars–Sun distances, which tends to reduce peak altitude, while observations at small solar zenith angles have low Mars–Sun distances, which tends to increase peak altitude, then observed values of peak altitude will change relatively little with observed solar zenith angle. The resultant value of L will be anomalously small and will not reflect the scale height of the neutral thermosphere at ionospheric altitudes. Two studies have found small values of L (Fox and Weber 2012; Fallows et al. 2015). Both used MGS radio occultation observations exclusively. However, solar zenith angle and Mars–Sun distance are not correlated in these observations. The magnitude of their correlation coefficient is 10^{-3} . For a visual confirmation of this lack of correlation, see Figure 8 of Withers et al. (2008).

Other hypotheses must be considered to explain why analyses of this large dataset have yielded anomalously small values of L . A distinctive feature of the MGS dataset is its narrow range of solar zenith angles: 70° to 90° . Examination of the bottom panel of Fig. 2 is informative. It shows that, at fixed solar zenith angle, there is much more scatter in the observed values of peak altitude at solar zenith angles greater than 80° than at solar zenith angles less than 70° . This is also apparent in Figure 6 of Peter et al. (2023). Thus the notion that, at fixed solar zenith angle, ionospheric peak altitude decreases with increasing Mars–Sun distance is satisfied much better at solar zenith angles less than 70° than at solar zenith angles greater than 80° . Therefore, we conclude that values of L of 5–7 km found by analyses of MGS observations at large solar zenith angles are not appropriate for extrapolation to the subsolar point. However, at solar zenith angles less than 70° , ionospheric peak altitude at fixed Mars–Sun distance does change with solar zenith angle approximately as expected from idealized theory with a lengthscale L that is comparable to the thermospheric scale height H .

Although not the outcome of a formal fit, there is one other instance of a small value of L . Earlier in this section, changes in the peak altitude values from the “not dusty” MAVEN ROSE data with solar zenith angle in the top panel of Fig. 2 were discussed. These observations, which were not classified by Mars–Sun distance in this panel, appeared to be represented well by the magenta line with $z_0 = 130$ km and $L = 5$ km. Unlike the MGS observations, these MAVEN ROSE observations extend to solar zenith angles smaller than 70° . In this instance, however, solar zenith angle and Mars–Sun distance are positively correlated (correlation coefficient of 0.33), which, as outlined above, will tend to lead to anomalously small values of L .

In summary, the change in peak altitude with solar zenith angle at fixed Mars–Sun distance is governed by

a lengthscale that is close to the thermospheric scale height, as expected. This is in contrast to some earlier results that suggested a significantly smaller lengthscale and weaker increase in peak altitude with increasing solar zenith angle. These earlier results were adversely affected by using near-terminator observations only, which display marked variability. Also, Figure 6 of Peter et al. (2023) and the bottom panel of Fig. 2 of this work suggest that the subsolar peak altitude changes between 120 km at aphelion and 140 km at perihelion. The concept of a single benchmark value for subsolar peak altitude is oversimplified.

5 M1 layer

Previous sections of this article have focused on the M2 layer of the ionosphere, where densities are greatest. Here we address the M1 layer, which lies beneath the M2 layer. Determination of layer peak density and altitude is straight-forward for the M2 layer, which is always a local maximum in electron density, but not for the M1 layer, whose morphology is more complex. Sometimes the M1 layer presents as a distinct local maximum, sometimes merely as a ledge or shoulder. It grows more prominent

as ionizing solar irradiance increases and the solar spectrum hardens (i.e., soft X-ray intensity increases relative to EUV intensity). Previous studies of the M1 layer have outlined the careful methods required to characterize its peak properties (Fallows et al. 2015; Fox and Yeager 2006; Fox et al. 2008). Efforts are currently underway to characterize the peak density and altitude of the MAVEN ROSE profiles. Those results will be reported in a separate publication once that project is complete. Instead, this article addresses one narrow, but fundamental, issue about the M1 layer: whether the M1 layer is present at small solar zenith angles or not.

Figure 3 shows that, although the M1 layer is a striking feature in many electron density profiles acquired by radio occultation experiments, it is notably absent from the two Viking Lander entry profiles at solar zenith angles of 44° and 45° (Hanson et al. 1977). Mayyasi and Mendillo (2015) suggested that the M1 layer is not present at these solar zenith angles, which would explain its absence from these observations. That is a significant statement. It predicts that the vertical structure of the Mars ionosphere is fundamentally different in the subsolar regions of the dayside ionosphere (one layer, M2 only) and in the near-terminator regions of the

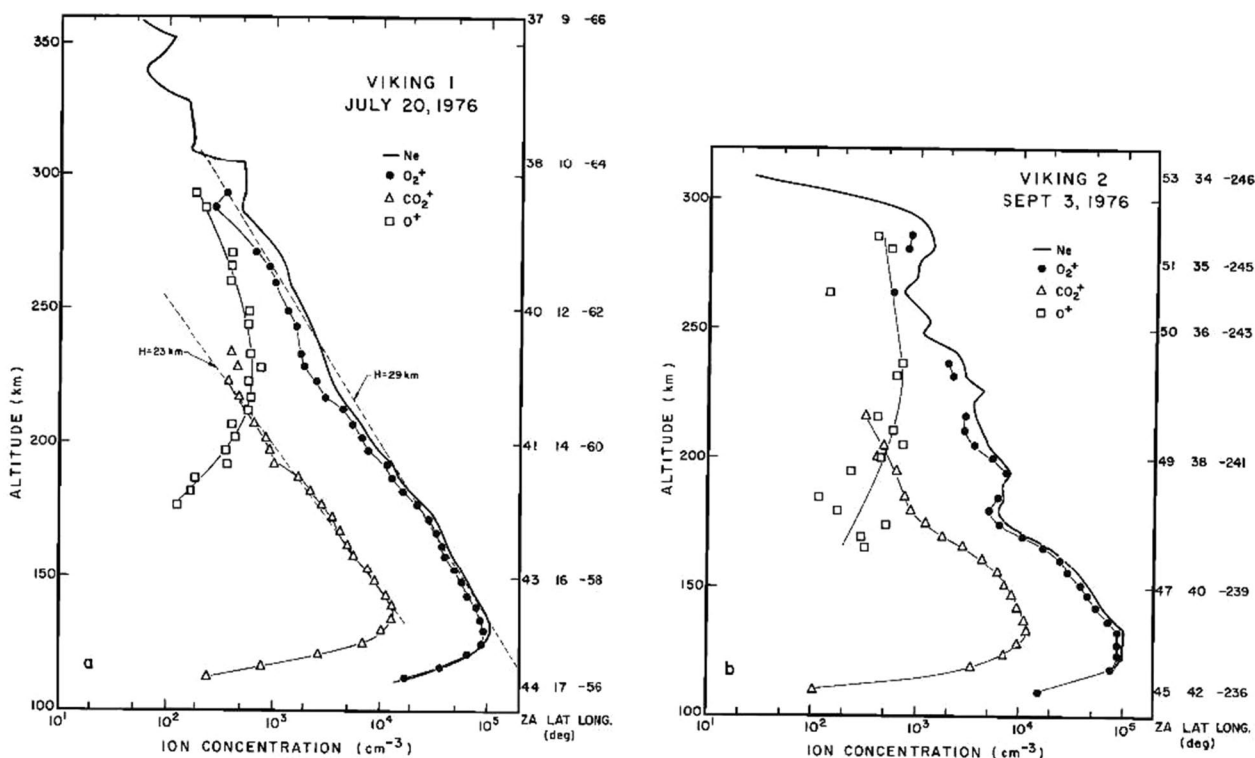


Fig. 3 Concentrations of O_2^+ , CO_2^+ and O^+ measured by retarding potential analyzers on the Viking 1 and 2 Landers. The solar zenith angle (degrees), latitude ($^{\circ}$ N) and longitude ($^{\circ}$ E) of each lander are shown to the right of each panel as functions of altitude. Reproduced with permission from Figure 6 of Hanson et al. (1977)

dayside ionosphere (two layers, M2 and M1). This would have profound consequences for the behavior of the ionosphere and its role in the wider Mars environment.

One set of radio occultation observations is particularly suited to comparisons with the Viking Lander profiles, which were acquired under solar minimum conditions when the monthly average of F10.7 was 70 and at solar zenith angles near 45° . Three spacecraft–spacecraft radio occultations between Mars Odyssey and Mars Reconnaissance Orbiter in September 2007 sampled similar solar zenith angles when the monthly average of F10.7 was also 70 (Ao et al. 2015). The equatorial latitudes of these observations are also similar to that of the Viking Lander 1 profile. Figure 4 shows these three profiles. The M1 layer is clearly visible in all three profiles, although it is most pronounced in the two profiles at solar zenith angles of 40.5° and 46.6° .

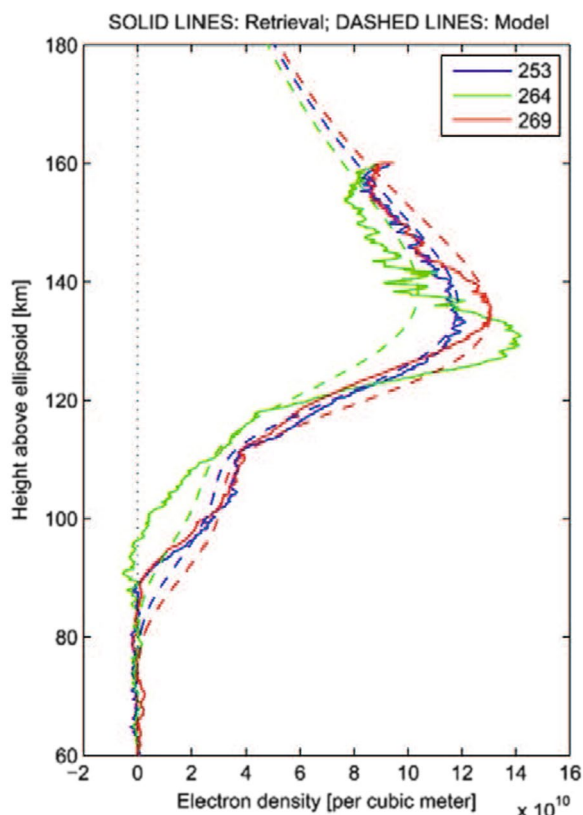


Fig. 4 Solid lines show electron density profiles measured by spacecraft–spacecraft radio occultations in 2007 under conditions that are directly comparable to those of the Viking Lander profiles. Dashed lines indicate model outputs that are not relevant in this work. The blue profile was acquired on day of year 253 (10 September) at a solar zenith angle of 46.6° . The green profile was acquired on day of year 264 (21 September) at a solar zenith angle of 53.2° . The red profile was acquired on day of year 269 (26 September) at a solar zenith angle of 40.5° . Reproduced with permission from the right panel of Figure 5 of Ao et al. (2015)

Examination of traditional spacecraft–Earth radio occultation observations reinforces the finding that the M1 layer is present at these solar zenith angles. As discussed above, there are 39 Mariner 9, 1 Viking Orbiter, and 3 MAVEN ROSE profiles at solar zenith angles less than 50° . Figure 5 shows a selected subset of the relevant Mariner 9 profiles, as well as all relevant Viking Orbiter and MAVEN ROSE profiles. The M1 layer is visible in most of these profiles, so it is not fundamentally absent at the solar zenith angles sampled by the two Viking Landers.

Solar zenith angle and solar irradiance considerations do not appear to explain why the Viking Landers did not observe an M1 layer in their ionospheric observations. Instead, the vertical range and resolution of the Viking Lander instruments may resolve this issue. Analysis of the M1 and M2 ionospheric layers using MGS radio occultation observations has found that the layers are separated by 25–30 km at solar zenith angles of 70° to 90° (Fallows et al. 2015). Similar analysis using Mariner 9 radio occultation observations from the primary mission at solar zenith angles of 47° – 57° found a similar result (Withers et al. 2015b). The Viking Lander measurements were acquired at altitudes of 110 km or greater and found the M2 layer at 125–130 km altitude (Hanson et al. 1977). We conclude that they do not extend to low enough altitudes to reach the peak of the M1 layer. In fact, this possibility was noted in the original report: the “data do not extend to low enough altitudes to observe the ledge in [electron density] detected by the occultation measurements near 100 km” (Hanson et al. 1977). Here “the ledge” refers to the M1 layer. Furthermore, the individual data points shown on Fig. 3 indicate a vertical resolution of 4 km or greater at the relevant altitudes. Even if the Viking Lander measurements did sample the topside of the M1 layer, then 4 or 5 coarsely separated points below the altitude of peak electron density in the M2 layer would not be sufficient to indicate an inflection or similar change in the vertical structure and thereby detect the presence of the M1 layer.

In summary, the M1 layer is a visible ionospheric feature at the solar irradiance and solar zenith angle conditions probed by the Viking Landers, but the vertical range and resolution of the Viking Lander instrument precluded detection of the M1 layer. The M1 layer remains a distinctive feature of the ionosphere of Mars down to solar zenith angles of 45° . Additional observations at smaller solar zenith angles would be required to test whether it remains significant to the subsolar point.

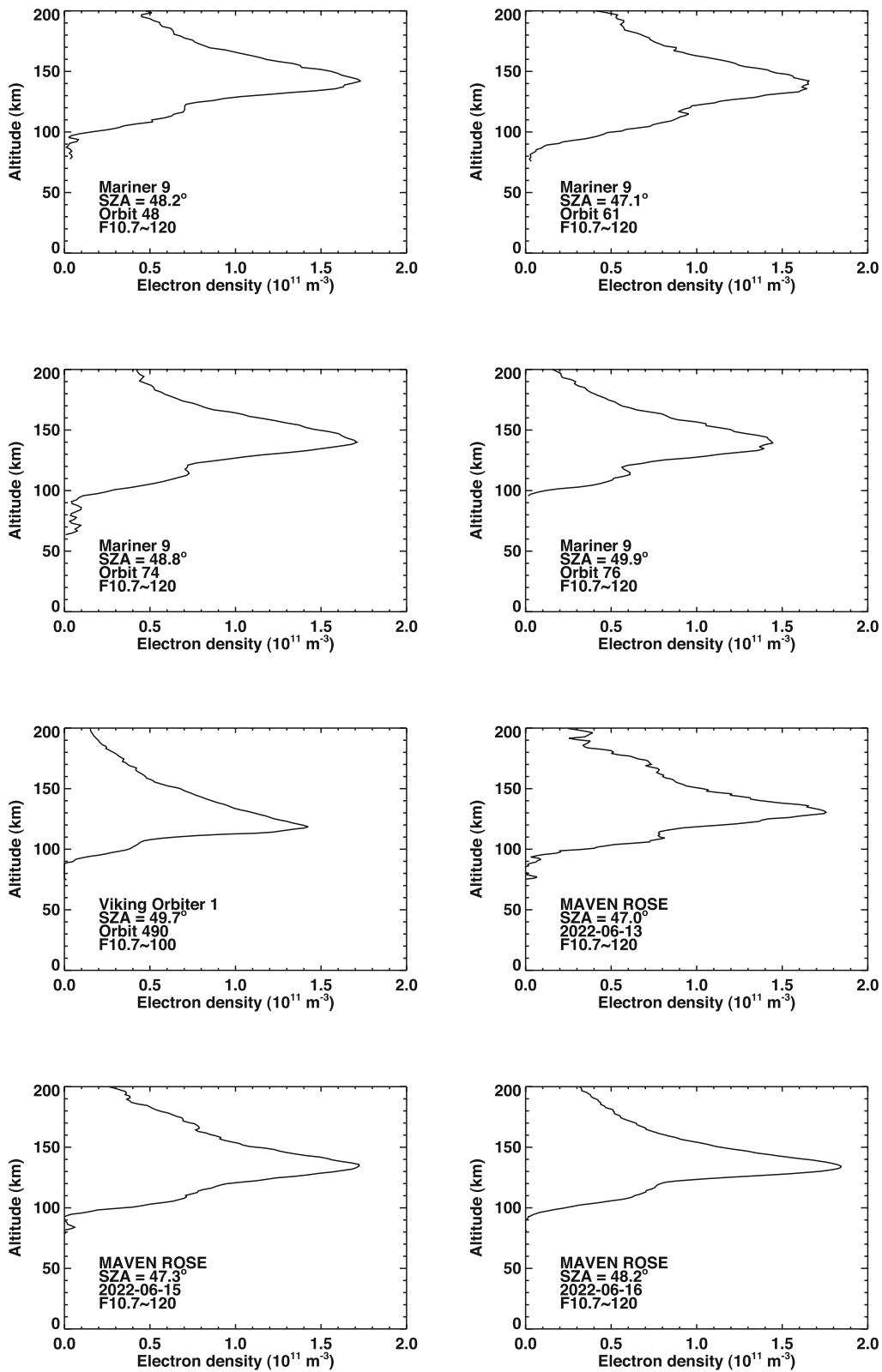


Fig. 5 Selected electron density profiles acquired by radio occultation instruments at solar zenith angles less than 50° . Spacecraft, solar zenith angle, monthly average F10.7, and either orbit number or date are indicated on each panel. In order to discriminate between the multiple MAVEN ROSE profiles acquired on a given day, note that the relevant UTC times are 19:35 on 13 June 2022, 04:00 on 15 June 2022, and 16:02 on 16 June 2022

6 Conclusions

It is technically challenging to determine the vertical structure of the ionosphere of Mars at small solar zenith angles. Geometric constraints limit spacecraft–Earth radio occultation observations at Mars to solar zenith angles between 45° and 135° . Current topside radar sounders have coarse altitude resolution that is greater than the thermospheric scale height and topside radar sounders fundamentally cannot sample below the peak of the M2 layer. In situ measurements from orbiting spacecraft are limited to altitudes above the spacecraft's periapsis. Spacecraft–spacecraft radio occultations would be an optimal way to measure the vertical structure of the ionosphere of Mars at small solar zenith angles, but such observations are rare, with only three having been published to date (Ao et al. 2015). Consequently, several basic questions about the ionosphere have not been resolved by previous work.

Based on changes in dayside peak electron density with solar zenith angle at solar zenith angle values accessible to radio occultations, we conclude that radio occultations indicate values for subsolar peak electron density consistent with those found by MARSIS: $1.53 \times 10^{11} \text{ m}^{-3}$ for F10.7=70 (solar minimum), $1.88 \times 10^{11} \text{ m}^{-3}$ for F10.7=120 (solar moderate), and $2.30 \times 10^{11} \text{ m}^{-3}$ for F10.7=200 (solar maximum). This agreement verifies that systematic errors do not affect peak density measurements from either type of instrument. Also, the seemingly small peak electron density values measured by the two Viking Landers under solar minimum conditions at solar zenith angles near 45° are consistent with the trends displayed by other peak electron density observations under solar minimum conditions and solar zenith angles of 55° – 90° . They are also consistent with comparable MARSIS observations. These values are reliable, which eliminates the troubling possibility that essentially all Mars ionospheric studies in the two decades between Viking and MGS are contaminated by a systematic error in absolute values of ion densities.

Based on changes in peak altitude with solar zenith angle at solar zenith angle values accessible to radio occultations, we find that the change in peak altitude with solar zenith angle is governed by a lengthscale that is close to the thermospheric scale height, as expected, in contrast to some earlier results that suggested a significantly smaller lengthscale and weaker increase in peak altitude with increasing solar zenith angle. However, this behavior is only apparent when the Mars–Sun distance is held fixed. As the subsolar peak altitude changes between 120 km at aphelion and 140 km at perihelion, erroneous results for this lengthscale may be obtained if peak altitude values from

a set of observations spanning a wide range of Mars–Sun distances are analyzed. We also find that the peak altitude at fixed Mars–Sun distance fluctuates more at near-terminator solar zenith angles than at smaller solar zenith angles. There are many possible factors that could account for this, including: the near-terminator peak occurring at higher altitudes and lower pressure levels, where the atmosphere is inherently more variable; the near-terminator region being affected by trans-terminator flows of plasma; and the assumption of spherical symmetry that is inherent to all limb-sounding observations being less applicable at near-terminator solar zenith angles.

Based on inspection of electron density profiles from radio occultation observations at solar zenith angles near 45° , we find that the M1 layer remains a distinctive feature of the ionosphere of Mars down to these solar zenith angles. The absence of the M1 layer from the two Viking Landers profiles acquired under solar minimum conditions at solar zenith angles near 45° should be attributed to the range and resolution of those observations, rather than to a fundamental change in the nature of the vertical structure of the ionosphere of Mars at small solar zenith angles.

If future spacecraft–spacecraft radio occultation observations are acquired, then it would be valuable to target them to the subsolar point and adjacent regions that cannot be accessed by spacecraft–Earth radio occultation observations. More observations of this type may be forthcoming from ESA's Mars Express and Trace Gas Orbiter spacecraft (Parrott, pers. comm.) Other observations, such as topside radar sounders or in situ instruments on orbiters, have limited vertical range and cannot measure down to the M1 layer.

Acknowledgements

We acknowledge helpful comments from several reviewers.

Author contribution

EB, DK, and KO acquired and processed the data. MF and JS contributed to discussions on the project. PW performed the project and wrote the article.

Funding

This work was supported, in part, by the MAVEN project, which is supported by NASA through the Mars Exploration Program.

Availability of data and materials

Mariner 9 profiles are available as supplemental information to Withers et al. (2015b) and at the PDS (https://pds-ppi.igpp.ucla.edu/mission/Mariner_9/MR9/RSS). Viking Orbiter profiles are available as supplemental information to Withers et al. (2020b) and at the PDS (https://atmos.nmsu.edu/data_and_services/atmospheres_data/voroelden/voroelden.html). MAVEN ROSE profiles are available from the PDS at <https://pds-ppi.igpp.ucla.edu/mission/MAVEN/MAVEN/ROSE>.

Declarations

Ethics approval and consent to participate

Not applicable.

Consent for publication

Not applicable.

Competing interests

The authors declare that they have no competing interests.

Author details

¹Department of Astronomy, Boston University, Boston, MA, USA. ²Center for Space Physics, Boston University, Boston, MA, USA. ³NASA Jet Propulsion Laboratory, Pasadena, CA, USA.

Received: 19 February 2024 Accepted: 19 June 2024

Published online: 15 July 2024

References

- Ambili KM, Tripathi KR, Choudhary RK, Imamura T (2022) On the origin and characteristic features of the V1 layer in Venus ionosphere using Akatsuki radio science experiment and the one-dimensional photochemical model. *Mon Not R Astron Soc* 516(4):5555–5562. <https://doi.org/10.1093/mnras/stac2624>
- Ambili KM, Choudhary RK, Tripathi KR (2024) On the role of minor neutrals in determining the characteristic features of the Venus ionosphere at low altitudes. *Mon Not R Astron Soc* 528(4):5601–5611. <https://doi.org/10.1093/mnras/stae339>
- Ao CO, Edwards CD, Kahan DS, Pi X, Asmar SW, Mannucci AJ (2015) A first demonstration of Mars crosslink occultation measurements. *Radio Sci* 50:997–1007. <https://doi.org/10.1002/2015RS005750>
- Barth CA, Stewart AIF, Bougher SW, Hunten DM, Bauer SJ, Nagy AF (1992) Aeronomy of the current martian atmosphere. In: Kieffer HH, Jakosky BM, Snyder CW, Matthews MS (eds) *Mars*. Arizona Press, Arizona, pp 1054–1089
- Bauer SJ, Lammer H (2004) *Planetary aeronomy*. Springer, New York
- Benna M, Mahaffy PR, Grebowsky JM, Fox JL, Yelle RV, Jakosky BM (2015) First measurements of composition and dynamics of the Martian ionosphere by MAVEN's Neutral Gas and Ion Mass Spectrometer. *Geophys Res Lett* 42:8958–8965. <https://doi.org/10.1002/2015GL066146>
- Bougher S, Jakosky B, Halekas J, Grebowsky J, Luhmann J, Mahaffy P, Connerney J, Eparvier F, Ergun R, Larson D, McFadden J, Mitchell D, Schneider N, Zurek R, Mazelle C, Andersson L, Andrews D, Baird D, Baker DN, Bell JM, Benna M, Brain D, Chaffin M, Chamberlin P, Chaufray J-Y, Clarke J, Collinson G, Combi M, Crary F, Cravens T, Crismani M, Curry S, Curtis D, Deignan J, Delory G, Dewey R, DiBraccio G, Dong C, Dong Y, Dunn P, Elrod M, England S, Eriksson A, Espley J, Evans S, Fang X, Fillingim M, Fortier K, Fowler CM, Fox J, Gröller H, Guzewich S, Hara T, Harada Y, Holsclaw G, Jain SK, Jolitz R, Leblanc F, Lee CO, Lee Y, Lefevre F, Lillis R, Livi R, Lo D, Ma Y, Mayyasi M, McClintock W, McNulty T, Modolo R, Montmessin F, Morooka M, Nagy A, Olsen K, Peterson W, Rahmati A, Ruhunusiri S, Russell CT, Sakai S, Sauvaud J-A, Seki K, Steckiewicz M, Stevens M, Stewart AIF, Stiepen A, Stone S, Tennishev V, Thiemann E, Tolson R, Toublanc D, Vogt M, Weber T, Withers P, Woods T, Yelle R (2015) Early MAVEN deep dip campaign reveals thermosphere and ionosphere variability. *Science* 350:0459. <https://doi.org/10.1126/science.aad0459>
- Bougher SW, Engel S, Hinson DP, Forbes JM (2001) Mars Global Surveyor Radio Science electron density profiles: neutral atmosphere implications. *Geophys Res Lett* 28:3091–3094. <https://doi.org/10.1029/2001GL012884>
- Bougher SW, Engel S, Hinson DP, Murphy JR (2004) MGS Radio Science electron density profiles: interannual variability and implications for the martian neutral atmosphere. *J Geophys Res* 109:E03010. <https://doi.org/10.1029/2003JE002154>
- Bougher SW, Brain DA, Fox JL, Francisco G-G, Simon-Wedlund C, Withers PG (2017) Upper neutral atmosphere and ionosphere. In: Haberle RM, Clancy RT, Forget F, Smith MD, Zurek RW (eds) *The atmosphere and climate of Mars*. Cambridge University Press, Cambridge, pp 405–432. <https://doi.org/10.1017/9781139060172.014>
- Chen Y, Liu L, Le H, Zhang H, Zhang R (2023) Evaluation for effects of variable Martian upper atmosphere on ionospheric peak electron density based on the MGS RO observation. *Icarus* 391:115364. <https://doi.org/10.1016/j.icarus.2022.115364>
- Cravens TE, Kliore AJ, Kozyra JU, Nagy AF (1981) The ionospheric peak on the Venus dayside. *J Geophys Res* 86(A13):11323–11329. <https://doi.org/10.1029/JA086iA13p11323>
- Fallows K, Withers P, Matta M (2015) An observational study of the influence of solar zenith angle on properties of the M1 layer of the Mars ionosphere. *J Geophys Res* 120:1299–1310. <https://doi.org/10.1002/2014JA020750>
- Felici M, Withers P, Smith MD, González-Galindo F, Oudrhiri K, Kahan D (2020) MAVEN ROSE Observations of the Response of the Martian Ionosphere to Dust Storms. *J Geophys Res* 125(6):e27083. <https://doi.org/10.1029/2019JA027083>
- Felici M, Withers P, Vogt MF, Hensley KG, Andersson L (2022) Electron densities in the ionosphere of mars: comparison of MAVEN/ROSE and MAVEN/LPW measurements. *J Geophys Res* 127(4):e30155. <https://doi.org/10.1029/2021JA030155>
- Fox JL, Kliore AJ (1997) Ionosphere: solar cycle variations. In: Bougher SW, Hunten DM, Phillips RJ (eds) *Venus II*. University of Arizona Press, Arizona, pp 161–188
- Fox JL, Weber AJ (2012) MGS electron density profiles: analysis and modeling of peak altitudes. *Icarus* 221:1002–1019. <https://doi.org/10.1016/j.icarus.2012.10.002>
- Fox JL, Yeager KE (2006) Morphology of the near-terminator martian ionosphere: a comparison of models and data. *J Geophys Res* 111:A10309. <https://doi.org/10.1029/2006JA011697>
- Fox JL, Yeager KE (2009) MGS electron density profiles: analysis of the peak magnitudes. *Icarus* 200:468–479. <https://doi.org/10.1016/j.icarus.2008.12.002>
- Fox JL, Galand MI, Johnson RE (2008) Energy deposition in planetary atmospheres by charged particles and solar photons. *Space Sci Rev* 139:3–62. <https://doi.org/10.1007/s11214-008-9403-7>
- Girazian Z, Withers P, Häusler B, Pätzold M, Tellmann S, Peter K (2015) Characterization of the lower layer in the dayside Venus ionosphere and comparisons with Mars. *Planet Space Sci* 117:146–158. <https://doi.org/10.1016/j.pss.2015.06.007>
- Golden-Marx E, Withers P, Kopf AJ (2021) The vertical extent of enhanced densities in cusp-like regions of the ionosphere of Mars. *J Geophys Res* 126(5):e28499. <https://doi.org/10.1029/2020JA028499>
- González-Galindo F (2020) Martian ionospheric observation and modelling. In: *Oxford Research Encyclopedia of Planetary Science*. p. 79. <https://doi.org/10.1093/acrefore/9780190647926.013.79>
- Gurnett DA, Kirchner DL, Huff RL, Morgan DD, Persoon AM, Averkamp TF, Duru F, Nielsen E, Safaeinili A, Plaut JJ, Picardi G (2005) Radar soundings of the ionosphere of Mars. *Science* 310:1929–1933. <https://doi.org/10.1126/science.1121868>
- Gurnett DA, Huff RL, Morgan DD, Persoon AM, Averkamp TF, Kirchner DL, Duru F, Akalin F, Kopf AJ, Nielsen E, Safaeinili A, Plaut JJ, Picardi G (2008) An overview of radar soundings of the martian ionosphere from the Mars Express spacecraft. *Adv Space Res* 41:1335–1346. <https://doi.org/10.1016/j.asr.2007.01.062>
- Haider SA, Mahajan KK, Kallio E (2011) Mars ionosphere: a review of experimental results and modeling studies. *Rev. Geophys.* 49(4):RG4001. <https://doi.org/10.1029/2011RG000357>
- Hanson WB, Sanatani S, Zuccaro DR (1977) The martian ionosphere as observed by the Viking retarding potential analyzers. *J Geophys Res* 82:4351–4363
- Hantsch MH, Bauer SJ (1990) Solar control of the Mars ionosphere. *Planet Space Sci* 38:539–542
- Hensley K, Withers P (2021) Response of Mars's topside ionosphere to changing solar activity and comparisons to Venus. *J Geophys Res* 126(3):e28913. <https://doi.org/10.1029/2020JA028913>
- Hinson DP, Simpson RA, Twicken JD, Tyler GL, Flasar FM (1999) Initial results from radio occultation measurements with Mars Global Surveyor. *J Geophys Res* 104:26997–27012
- Jakosky BM, Lin RP, Grebowsky JM, Luhmann JG, Mitchell DF, Beutelschies G, Priser T, Acuna M, Andersson L, Baird D, Baker D, Bartlett R, Benna M, Bougher S, Brain D, Carson D, Cauffman S, Chamberlin P, Chaufray J-Y, Cheatom O, Clarke J, Connerney J, Cravens T, Curtis D, Delory G, Demcak S, DeWolfe A, Eparvier F, Ergun R, Eriksson A, Espley J, Fang X, Folta D, Fox J, Gomez-Rosa C, Habenicht S, Halekas J, Holsclaw G, Houghton M, Howard R, Jarosz M, Jedrich N, Johnson M, Kasprzak W, Kelley M, King T, Lankton M, Larson D, Leblanc F, Lefevre F, Lillis R, Mahaffy P, Mazelle C, McClintock W, McFadden J, Mitchell DL, Montmessin F, Morrissey J,

- Peterson W, Possel W, Sauvaud J-A, Schneider N, Sidney W, Sparacino S, Stewart AIF, Tolson R, Toubanc D, Waters C, Woods T, Yelle R, Zurek R (2015) The Mars atmosphere and volatile evolution (MAVEN) mission. *Space Sci Rev* 195:3–48. <https://doi.org/10.1007/s11214-015-0139-x>
- Kliore AJ (1992) Radio occultation observations of the ionospheres of Mars and Venus. *Venus and Mars: atmospheres, ionospheres, and solar wind interactions*, Geophysical Monograph Series, vol 66. American Geophysical Union, Washington, DC, pp 265–276
- Kliore AJ, Cain DL, Fjeldbo G, Seidel BL, Sykes MJ, Rasool SI (1972) The atmosphere of Mars from Mariner 9 radio occultation measurements. *Icarus* 17:484–516
- Kliore AJ, Fjeldbo G, Seidel BL, Sykes MJ, Woiceshyn PM (1973) S band radio occultation measurements of the atmosphere and topography of Mars with Mariner 9: extended mission coverage of polar and intermediate latitudes. *J Geophys Res* 78:4331–4351. <https://doi.org/10.1029/JB078i020p04331>
- Liao H-R, Wang J-S, Zou H, Wang X-D (2006) Observational features of the secondary layer of the Martian ionosphere. *Adv Geosci* 3:135–143. https://doi.org/10.1142/9789812707192_0014
- Lindal GF, Hotz HB, Sweetnam DN, Shippony Z, Hartsell GV, Spear RT (1979) Viking radio occultation measurements of the atmosphere and topography of Mars—data acquired during 1 Martian year of tracking. *J Geophys Res* 84:8443–8456. <https://doi.org/10.1029/JB084iB14p08443>
- Luhmann JG, Tatrallyay M, Pepin RO (1992) Venus and Mars: atmospheres, ionospheres, and solar wind interactions. *American Geophysical Union Geophysical Monograph Series*
- Mayyasi M, Mendillo M (2015) Why the Viking descent probes found only one ionospheric layer at Mars. *Geophys Res Lett* 42(18):7359–7365. <https://doi.org/10.1002/2015GL065575>
- Mendillo M, Narvaez C, Vogt MF, Mayyasi M, Forbes J, Galand M, Thiemann E, Benna M, Eparvier F, Chamberlin P, Mahaffy P, Andersson L (2017) Sources of ionospheric variability at Mars. *J Geophys Res* 122(9):9670–9684. <https://doi.org/10.1002/2017JA024366>
- Mendillo M, Narvaez C, Trovato J, Withers P, Mayyasi M, Morgan D, Kopf A, Gurnett D, Němec F, Campbell B (2018) Mars Initial Reference Ionosphere (MIRI) model: updates and validations using MAVEN, MEX, and MRO data sets. *J Geophys Res* 123(7):5674–5683. <https://doi.org/10.1029/2018JAO25263>
- Morgan DD, Gurnett DA, Kirchner DL, Fox JL, Nielsen E, Plaut JJ (2008) Variation of the Martian ionospheric electron density from Mars Express radar soundings. *J Geophys Res* 113:A09303. <https://doi.org/10.1029/2008JAO13313>
- Morgan DD, Witasse O, Nielsen E, Gurnett DA, Duru F, Kirchner DL (2013) The processing of electron density profiles from the Mars Express MARSIS topside sounder. *Radio Sci* 48(3):197–207. <https://doi.org/10.1002/rds.20023>
- Mukundan V, Withers P, González-Galindo F, Thampai SV, Bhardwaj A, Felici M (2022) Atypically intense and delayed response of the Martian ionosphere to the regional dust storm of 2016: a study using MAVEN observations and models. *J. Geophys. Res.* 127(12):e2022JE007645. <https://doi.org/10.1029/2022JE007645>
- Nielsen E (2004) Mars express and MARSIS. *Space Sci Rev* 111(1):245–262. <https://doi.org/10.1023/B:SPAC.0000032712.05204.5e>
- Nielsen E, Zou H, Gurnett DA, Kirchner DL, Morgan DD, Huff R, Orosei R, Safa-inili A, Plaut JJ, Picardi G (2006) Observations of vertical reflections from the topside Martian ionosphere. *Space Sci Rev.* 126:373–388. <https://doi.org/10.1007/s11214-006-9113-y>
- Němec F, Morgan DD, Gurnett DA, Duru F, Truhlík V (2011) Dayside ionosphere of Mars: empirical model based on data from the MARSIS instrument. *J Geophys Res* 116:E07003. <https://doi.org/10.1029/2010JE003789>
- Němec F, Morgan DD, Gurnett DA (2016) On improving the accuracy of electron density profiles obtained at high altitudes by the ionospheric sounder on the Mars Express spacecraft. *J Geophys Res* 121(10):10117–10129. <https://doi.org/10.1002/2016JA023054>
- Němec F, Morgan DD, Kopf AJ, Gurnett DA, Pitoňák D, Fowler CM, Andrews DJ, Andersson L (2019) Characterizing average electron densities in the Martian dayside upper ionosphere. *J Geophys Res* 124(1):76–93. <https://doi.org/10.1029/2018JE005849>
- Pätzold M, Häusler B, Tyler GL, Andert T, Asmar SW, Bird MK, Dehant V, Hinson DP, Rosenblatt P, Simpson RA, Tellmann S, Withers P, Beuthe M, Efimov AI, Hahn M, Kahan D, Le Maistre S, Oschlisniok J, Peter K, Remus S (2016) Mars Express 10 years at Mars: observations by the Mars Express Radio Science Experiment (MaRS). *Planet Space Sci* 127:44–90. <https://doi.org/10.1016/j.pss.2016.02.013>
- Peter K, Pätzold M, Molina-Cuberos G, Witasse O, González-Galindo F, Withers P, Bird MK, Häusler B, Hinson DP, Tellmann S, Tyler GL (2014) The dayside ionospheres of Mars and Venus: Comparing a one-dimensional photochemical model with MaRS (Mars Express) and VeRa (Venus Express) observations. *Icarus* 233:66–82. <https://doi.org/10.1016/j.icarus.2014.01.028>
- Peter K, Pätzold M, Molina-Cuberos GJ, González-Galindo F, Witasse O, Tellmann S, Häusler B, Bird MK (2021) The lower dayside ionosphere of Mars from 14 years of MaRS radio science observations. *Icarus* 359:114213. <https://doi.org/10.1016/j.icarus.2020.114213>
- Peter K, Pätzold M, Montabone L, Thiemann E, González-Galindo F, Witasse O, Tellmann S, Bird MK (2023) The effects of atmospheric dust and solar radiation on the dayside ionosphere of Mars derived from 17 years of Mars Express radio science observations. *Icarus* 400:115565. <https://doi.org/10.1016/j.icarus.2023.115565>
- Schunk RW, Nagy AF (2009) *Ionospheres*, 2nd edn. Cambridge Univ. Press, New York
- Simon Wedlund C, Gronoff G, Liliensten J, Ménager H, Barthélemy M (2011) Comprehensive calculation of the energy per ion pair or W values for five major planetary upper atmospheres. *Ann Geophys* 29:187–195. <https://doi.org/10.5194/angeo-29-187-2011>
- Stewart AIF, Hanson WB (1982) Mars' upper atmosphere: mean and variations. *Adv Space Res* 2:87–101. [https://doi.org/10.1016/0273-1177\(82\)90109-0](https://doi.org/10.1016/0273-1177(82)90109-0)
- Stone SW, Yelle RV, Benna M, Elrod MK, Mahaffy PR (2018) Thermal structure of the Martian upper atmosphere from MAVEN NGIMS. *J Geophys Res* 123(11):2842–2867. <https://doi.org/10.1029/2018JE005559>
- Stone SW, Yelle RV, Benna M, Elrod MK, Mahaffy PR (2022) Neutral composition and horizontal variations of the Martian upper atmosphere from MAVEN NGIMS. *J Geophys Res* 127(6):e07085. <https://doi.org/10.1029/2021JEO07085>
- Tamburo P, Withers P, Dalba PA, Moore L, Koskinen T (2023) Cassini radio occultation observations of Saturn's ionosphere: electron density profiles from 2005 to 2013. *J Geophys Res* 128(4):e2023JA031310. <https://doi.org/10.1029/2023JA031310>
- Tripathi KR, Choudhary RK, Ambili KM, Imamura T (2023) Venusian ionosphere during deep solar minima: some new insights using Akatsuki Radio Science Experiment. *J Geophys Res* 128(4):e2023JE007768. <https://doi.org/10.1029/2023JE007768>
- Tyler GL, Balmino G, Hinson DP, Sjogren WL, Smith DE, Simpson RA, Asmar SW, Priest P, Twicken JD (2001) Radio science observations with Mars Global Surveyor: orbit insertion through one Mars year in mapping orbit. *J Geophys Res* 106:23327–23348. <https://doi.org/10.1029/2000JE001348>
- Vogt MF, Withers P, Fallows K, Flynn CL, Andrews DJ, Duru F, Morgan DD (2016) Electron densities in the ionosphere of Mars: a comparison of MARSIS and radio occultation measurements. *J Geophys Res* 121(10):10241–10257. <https://doi.org/10.1002/2016JA022987>
- Vogt MF, Withers P, Fallows K, Andersson L, Girazian Z, Mahaffy PR, Benna M, Elrod MK, Connerney JEP, Easley JR, Eparvier FG, Jakosky BM (2017) MAVEN observations of dayside peak electron densities in the ionosphere of Mars. *J Geophys Res* 122:891–906. <https://doi.org/10.1002/2016JA023473>
- Witasse O, Cravens T, Mendillo M, Moses J, Kliore A, Nagy AF, Breus T (2008) Solar system ionospheres. *Space Sci Rev.* 139:235–265. <https://doi.org/10.1007/s11214-008-9395-3>
- Withers P (2006) Mars Global Surveyor and Mars Odyssey Accelerometer observations of the Martian upper atmosphere during aerobraking. *Geophys Res Lett* 33:L02201. <https://doi.org/10.1029/2005GL024447>
- Withers P (2009) A review of observed variability in the dayside ionosphere of Mars. *Adv Space Res* 44:277–307. <https://doi.org/10.1016/j.asr.2009.04.027>
- Withers P, Mendillo M, Hinson DP, Cahoy K (2008) Physical characteristics and occurrence rates of meteoric plasma layers detected in the Martian ionosphere by the Mars Global Surveyor Radio Science Experiment. *J Geophys Res* 113:A12314. <https://doi.org/10.1029/2008JA013636>
- Withers P, Morgan DD, Gurnett DA (2015) Variations in peak electron densities in the ionosphere of Mars over a full solar cycle. *Icarus* 251:5–11. <https://doi.org/10.1016/j.icarus.2014.08.008>

- Withers P, Weiner S, Ferreri NR (2015) Recovery and validation of Mars ionospheric electron density profiles from Mariner 9. *Earth Planets and Space* 67:194. <https://doi.org/10.1186/s40623-015-0364-2>
- Withers P, Felici M, Mendillo M, Moore L, Narvaez C, Vogt MF, Jakosky BM (2018) First ionospheric results from the MAVEN Radio Occultation Science Experiment (ROSE). *J Geophys Res* 123:4171–4180. <https://doi.org/10.1029/2018JA025182>
- Withers P, Felici M, Mendillo M, Moore L, Narvaez C, Vogt MF, Oudrhiri K, Kahan D, Jakosky BM (2020) The MAVEN Radio Occultation Science Experiment (ROSE). *Space Sci Rev* 216(4):61. <https://doi.org/10.1007/s11214-020-00687-6>
- Withers P, Felici M, Flynn C, Vogt MF (2020) Recovery and validation of Mars ionospheric electron density profiles from Viking orbiter radio occultation observations. *Planet Sci J* 1(1):14. <https://doi.org/10.3847/PSJ/ab8fb2>
- Withers P, Felici M, Mendillo M, Vogt MF, Barbinis E, Kahan D, Oudrhiri K, Gray C, Lee CO, Xu S, Lester M, Sanchez-Cano B, Jakosky BM, Curry S (2022) Observations of high densities at low altitudes in the nightside ionosphere of Mars by the MAVEN Radio Occultation Science Experiment (ROSE). *J Geophys Res* 127(11):e2022JA030737. <https://doi.org/10.1029/2022JA030737>
- Withers P, Felici M, Hensley K, Mendillo M, Barbinis E, Kahan D, Oudrhiri K, Girazian Z (2023) The ionosphere of Mars from solar minimum to solar maximum: dayside electron densities from MAVEN and Mars Global Surveyor radio occultations. *Icarus* 393:114508. <https://doi.org/10.1016/j.icarus.2021.114508>
- Yao M, Cui J, Wu X, Huang Y, Wang W (2019) Variability of the Martian ionosphere from the MAVEN Radio Occultation Science Experiment. *Earth Planet Phys* 3:283–289. <https://doi.org/10.26464/epp2019029>
- Zhang MHG, Luhmann JG, Kliore AJ, Kim J (1990) A post-Pioneer Venus reassessment of the martian dayside ionosphere as observed by radio occultation methods. *J Geophys Res* 95:14829–14839
- Zurek RW, Tolson RA, Bougher SW, Lugo RA, Baird DT, Bell JM, Jakosky BM (2017) Mars thermosphere as seen in MAVEN accelerometer data. *J Geophys Res* 122(3):3798–3814. <https://doi.org/10.1002/2016JA023641>

Publisher's Note

Springer Nature remains neutral with regard to jurisdictional claims in published maps and institutional affiliations.